The Astrophysical Journal, 571:366–377, 2002 May 20

AUSTRALIA TELESCOPE COMPACT ARRAY RADIO IMAGING OF THE PROPLYD-LIKE OBJECTS IN THE GIANT H II REGION NGC 3603

A. Mücke,[1] B. S. Koribalski,[2] A. F. J. Moffat,[1] M. F. Corcoran,[3] and I. R. Stevens[4]

Received 2001 January 16; accepted 2002 January 24

ABSTRACT

Three cometary-shaped objects in the giant H II region NGC 3603, originally found and identified as proto–planetary disks (proplyds) by Brandner and coworkers using the *Hubble Space Telescope* and the Very Large Telescope in the optical and near-infrared, have been detected with the Australia Telescope Compact Array[5] in the radio continuum at 3 and 6 cm. All three proplyd-like objects are clearly resolved with an extent of a few arcseconds. The integrated 6 cm fluxes are up to 1.3 times higher than the 3 cm fluxes with spectral indices averaged over the whole clump between $\alpha = -0.1$ and -0.5 ($S_\nu \propto \nu^\alpha$), indicating the likely presence of nonthermal emission in at least some of the sources. We present spectral-index maps and show that the sites of negative radio spectral indices are predominantly concentrated in the direction of the tails in at least two of the three proplyd-like nebulae, while positive spectral indices are found in the region facing the ionizing star cluster. We propose that thermal bremsstrahlung and nonthermal synchrotron radiation are at work in all three proplyd-like sources. In at least one of the three objects, optically thin nonthermal synchrotron emission appears to dominate when averaged over its whole spatial extent, while the spectrum of a second source shows a marginal indication of a nonthermal spectrum. The average spectrum of the third source is in agreement with thermal bremsstrahlung. All measured fluxes are at least one order of magnitude higher than those predicted by Brandner and coworkers. Upper limits for mass-loss rates due to photoevaporation are calculated to be $\sim 10^{-5}\ M_\odot\ \mathrm{yr}^{-1}$ and for electron densities to be $\sim 10^4\ \mathrm{cm}^{-3}$. Due to the unexpectedly large radio luminosities of the proplyd-like features and because the radio emission is extended, a (proto-) stellar origin of the nonthermal emission from a dust enshrouded star appears unlikely. Instead, we propose that magnetized regions within the envelope of the proplyd-like nebulae exist.

Subject headings: H II regions — ISM: individual (NGC 3603) — radio continuum: ISM — stars: early-type — stars: formation — stars: pre–main-sequence

1. INTRODUCTION

The giant H II region NGC 3603, located at a distance of about 6 kpc, shows the densest concentration and largest collection of visible massive stars known in our Galaxy. Recent *Hubble Space Telescope* (*HST*) images of $\sim 0\farcs2$ angular resolution (Moffat, Drissen, & Shara 1994) have shown that NGC 3603 consists of three Wolf-Rayet (WR) stars and ~70 O-type stars, with an estimated 40–50 of these stars located in the central $\sim 30'' \times 30''$ (1 pc × 1 pc) region. The three H-rich WR stars of subtype WNL are also located within $\sim 1''$ of each other in the central core and are the brightest members of the cluster. They are believed to be massive main-sequence stars that, like the bright stars in R136a, drive very strong winds (De Koter, Heap, & Hubeny 1997; Crowther & Dessart 1998). NGC 3603 has also been shown to be a seat of active star formation outside the main cluster region (e.g., Brandner et al. 2000). In particular, three distinct dense cometary nebulae were detected there using *HST* and the Very Large Telescope (VLT): Are these ultracompact H II regions (UCHRs) or proto–planetary disks (proplyds)?

UCHRs are small (less than 0.1 pc) nebulae, *internally* photoionized by a deeply embedded, massive star. Even though the embedded stars are very luminous, they are invisible at optical wavelengths because of the surrounding dust; instead, they show strong far-infrared emission. Their radio-continuum emission is often associated with OH and H_2O masers. The morphology of UCHRs in high-resolution radio-continuum images ranges over spherical, cometary, core-halo, shell, and irregular (Wood & Churchwell 1989).

In contrast, a proplyd is a phenomenon describing a low-mass young stellar object (YSO) with a circumstellar disk, embedded in a dense (neutral and ionized) envelope that is being *externally* photoevaporated by the ultraviolet radiation from one or more massive stars. These low-mass stars are not able to ionize their surroundings significantly. The disks in these systems are either observed directly (as in Orion, where the disks are seen directly or in silhouette against the bright background nebula; Bally, O'Dell, & McCaughrean 2000) or inferred because in almost all the proplyds, (young) low-mass stars are visible at optical or near-infrared (NIR) wavelengths (see, e.g., Stecklum et al. 1998). At low angular resolution, proplyds look like UCHRs, but at high resolution, optical and NIR images reveal their different nature. Therefore, most proplyds would have been classified as UCHRs prior to those observations. In some cases, the distinction between the two classes remains difficult. Given the fact that there are about

[1] Département de Physique, Université de Montréal, CP 6128, Succ. Centre-Ville, Montreal, QC H3C 3J7, Canada; Observatoire du Mont Mégantic; A. M. now at Institut für Theoretische Physik, Ruhr-Universität Bochum, Lehrstuhl IV, Weltraum- und Astrophysik, D-44780 Bochum, Germany; afm@tp4.ruhr-uni-bochum.de, moffat@astro.umontreal.ca.

[2] Australia Telescope National Facility, CSIRO, P.O. Box 76, Epping 1710, Australia; baerbel.koribalski@atnf.csiro.au.

[3] Goddard Space Flight Center, NASA Code 661, Laboratory for High Energy Astrophysics, Greenbelt, MD 20771; corcoran@barnegat.gsfc.nasa.gov.

[4] School of Physics and Astronomy, University of Birmingham, Birmingham B15 2TT, UK; irs@star.sr.bham.ac.uk.

[5] The Australia Telescope is funded by the Commonwealth of Australia for operation as a National Facility managed by CSIRO.

4 times more UCHRs than expected (Churchwell 1990) from star formation rates and given the potential problems identifying host stars for UCHRs (e.g., some may not have enough far-infrared flux to account for an internal OB star), it may well be that a large fraction of cataloged UCHRs are misidentified proplyds. Interferometric radio-continuum observations of proplyds are needed to determine their structure and spectral indices, and thus the nature of their emission, as well as mass-loss rates and extinctions when compared with measured Hα fluxes.

Proplyds were first identified in the Orion Nebula,[6] where over 150 of them are known (O'Dell, Wen, & Hu 1993). Two proplyds have been identified in more distant nebulae: one in NGC 2024 by Stapelfeldt et al. (1997) and one, G5.97−1.17, in the Lagoon Nebula by Stecklum et al. (1998). The three proplyd-like objects, hereafter referred to as P1, P2, and P3, in NGC 3603 (Brandner et al. 2000) are the biggest, youngest, and most massive ones found *so far*. They are also the most distant known. These emission nebulae are clearly resolved in the *HST*/WFPC2 observations and share the overall morphology of the proplyds in Ori. All three nebulae are rim brightened and teardrop shaped with the tails pointing away from the central ionizing cluster.

According to Brandner et al. (2000), the brightest object (P1), which has a projected distance of 1.3 pc from the cluster, has the spectral (excitation) characteristics of a UCHR. Optical spectra reveal the presence of an underlying, heavily reddened continuum source, which is also confirmed by NIR VLT/ISAAC observations. The WFPC2 observations show that only the outermost layer is ionized, whereas the interior is neutral. The morphology of P1 is described as a heart-shaped head with a collimated structure in between, which can be understood as the superposition of two individual proplyds. In contrast, P2 and P3, located at projected distances of 2.2 and 2.0 pc from the stellar cluster, respectively, show approximately axisymmetric morphologies. No embedded disk or central star has been detected so far in any of these nebulae, preventing a clear identification as proplyds. The optical point source (see Fig. 2, *top right*) close to P3 is probably not physically linked to the nebula (Brandner et al. 2000). The proplyd-like structures in NGC 3603 are about 2 orders of magnitude fainter than typical UCHRs but have a typical extent of 9000 AU with tails extending to 21,000 AU, much larger in size than the proplyds in Ori.

Recent 3.4 cm radio-continuum and recombination-line measurements of NGC 3603 by De Pree, Nysewander, & Goss (1999),which were focused on abundance measurements and the bright continuum emission from the ionized gas in this region, have an angular resolution of $\sim 7''$ and a 5 σ sensitivity of 55 mJy. By obtaining high-sensitivity and high angular resolution ($\sim 1''$–$2''$) Australia Telescope Compact Array (ATCA) observations, we primarily aimed to study the radio emission of the winds from many of the early-type stars in the cluster, as well as to detect and resolve the proplyd-like objects and other gaseous regions in the cluster periphery. This paper focuses on the proplyd-like sources[7] only, which have been detected and are shown to be clearly resolved with the ATCA. A subsequent paper containing a detailed study of the whole NGC 3603 region based on our ATCA observations will follow.

2. OBSERVATIONS AND DATA REDUCTION

Radio-continuum observations of NGC 3603 were made with the ATCA in the 6A, 6B, 6C, and 6D configurations in five observing runs in 2000 February, April, June, September, and November, with a total of 60 hr assigned observing time. The observing frequencies were 4.8 (6 cm) and 8.64 GHz (3 cm), with a bandwidth in each case of 128 MHz. Detailed observing parameters are given in Table 1. The three data sets were combined, reduced, and analyzed in MIRIAD using standard procedures. The full Stokes parameters were measured. The flux density scale was calibrated using observations of the primary calibrator 1934−638 assuming flux densities of 2.84 and 5.83 Jy at 3 and 6 cm, respectively.

A primary beam correction was carried out. To obtain high angular resolution and filter the extended emission to emphasize the small-scale structure, we used uniform weighting of the *u*-*v* data while omitting the shortest baselines, up to 25 kλ. We find that for a 25 kλ cutoff, all bright extended nebula emission is removed from the proplyd-like objects, even at 6 cm. Figure 1 shows an example of a combined 3 cm radio map where a *u*-*v* cut of 10 kλ was chosen. A zoom on the three proplyd-like objects is shown in Figure 2. For the 6 cm maps, a *u*-*v* cut of 25 kλ was used. The average rms in these combined radio maps is approximately 0.2 mJy at 3 cm and 0.4 mJy at 6 cm but varies throughout the map. The rms levels near the proplyd-like objects, which lie in rather empty regions, are $\sim$0.1 mJy at 3 cm and $\sim$0.2 mJy at 6 cm. The dynamic range in the 3 and 6 cm images is about 1:100. Fitting a two-dimensional Gaussian to the dirty beam gives FWHM values of $0\farcs94 \times 0\farcs77$ to $1\farcs06 \times 0\farcs87$ at 3 cm and $1\farcs53 \times 1\farcs23$ to $1\farcs83 \times 1\farcs49$ at 6 cm, depending on the *u*-*v* cut employed. In Figure 2 we have restored the cleaned maps with a circular Gaussian beam of width $1''$ at 3 cm and $2''$ at 6 cm.

To create spectral-index maps between 3 and 6 cm, we convolved the 3 cm map with a Gaussian appropriate for achieving the resolution of the beam FWHM at 6 cm. The spectral-index maps were then derived from the 6 cm and convolved 3 cm maps using a clip value of 1.0 mJy beam^{-1}, corresponding to approximately 10 σ at 3 cm and 5 σ at 6 cm (statistical errors). Error maps for the spectral-index maps were calculated using error propagation. We note, however, that spectral indices of extended sources as obtained from interferometric data have to be regarded with caution.

[6] There are a variety of different terms used in the literature for describing the knots of ionized gas in M42 (Ori): e.g., CKs (cometary knots), PIGs (partially ionized globules), EIDERS (external ionized [accretion] disks in the environs of radiation sources), and proplyds (proto–planetary disks); for a summary, see McCullough et al. (1995). Another expression being used is EGGs (evaporating gaseous globules), describing the objects found in M16 (Eagle Nebula). The cometary knots found in the Helix Nebula are compact globules and very different from proplyds, as they contain no stars.

[7] Throughout this paper we use the term "proplyd-like" for these cometary-shaped objects in NGC 3603, since the identification of these objects as true proplyds is premature, owing to the lack of a clear detection of a central disk or star.

TABLE 1

OBSERVING PARAMETERS

PARAMETER	DATE (LOCAL TIME)				
	Feb 9–10	Apr 8–9	Jun 19	Sep 13–14	Nov 8–9
Configurations	6A	6D	6B	6A	6C
Time on source (minutes)	561	514	480	513	543
R.A. (J2000.0)	11 15 07	11 15 07	11 15 07	11 15 07	11 15 07
decl. (J2000.0)	−61 16 00	−61 16 00	−61 16 00	−61 16 00	−61 16 00
Total bandwidth (MHz)	128	128	128	128	128
Number of channels	32	32	32	32	32
Frequencies (MHz)	8640, 4800	8640, 4800	8640, 4800	8640, 4800	8640, 4800
Beam size at 3 cm (arcsec^2)	$\sim 1 \times 1$	$\sim 1 \times 1$	$\sim 1 \times 1$	$\sim 1 \times 1$	$\sim 1 \times 1$
Beam size at 6 cm (arcsec^2)	$\sim 2 \times 2$	$\sim 2 \times 2$	$\sim 2 \times 2$	$\sim 2 \times 2$	$\sim 2 \times 2$
Average rms near proplyds at 3 cm (mJy beam^{-1})	~0.1	~0.1	~0.1	~0.1	~0.1
Average rms near proplyds at 6 cm (mJy beam^{-1})	~0.2	~0.2	~0.2	~0.2	~0.2
Flux calibrator	1934−63	1934−63	1934−63	1934−63	1934−63
Phase calibrator	1059−63	1059−63	1059−63	1059−63	1059−63

NOTE.—Units of right ascension are hours, minutes, and seconds, and units of declination are degrees, arcminutes, and arcseconds.

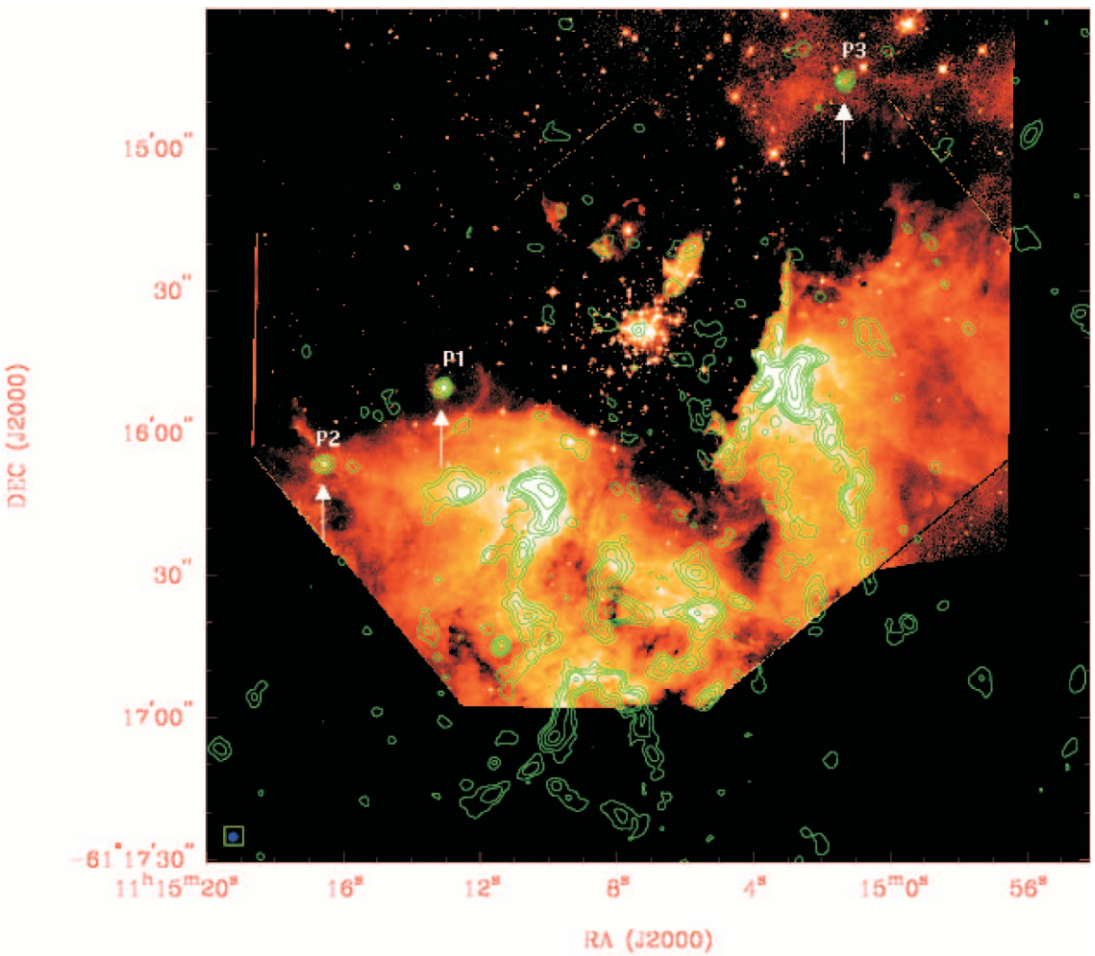

FIG. 1.—Plot of 3 cm continuum map with a *u-v* cutoff at 10 kλ of NGC 3603 overlaid onto the Hα and broadband *HST* image from Brandner et al. (2000). Note that in this radio map, the small-scale structure is emphasized because of our chosen *u-v* cutoff in the data analysis. For smoothing purposes, the map was restored with a $2'' \times 2''$ beam size. The brightest extended continuum regions correspond to the heads of the giant gaseous pillars, showing evidence for the interaction of ionizing radiation with cold molecular hydrogen clouds. The radio emission from IRS 9, a deeply enshrouded association of protostars at the foot of the southeastern pillar, will be discussed in a forthcoming paper (Mücke et al., in preparation). The three nebulae indicated are the proplyd-like sources; their tadpole shape is shown in Fig. 2. The contour levels at 3 cm are −0.8, 0.8, 2.0, 4.0, 6.0, 12.0, 24, and 48 mJy beam^{-1}. The beam is shown inside the box at the bottom left corner. North is to the top and east to the left.

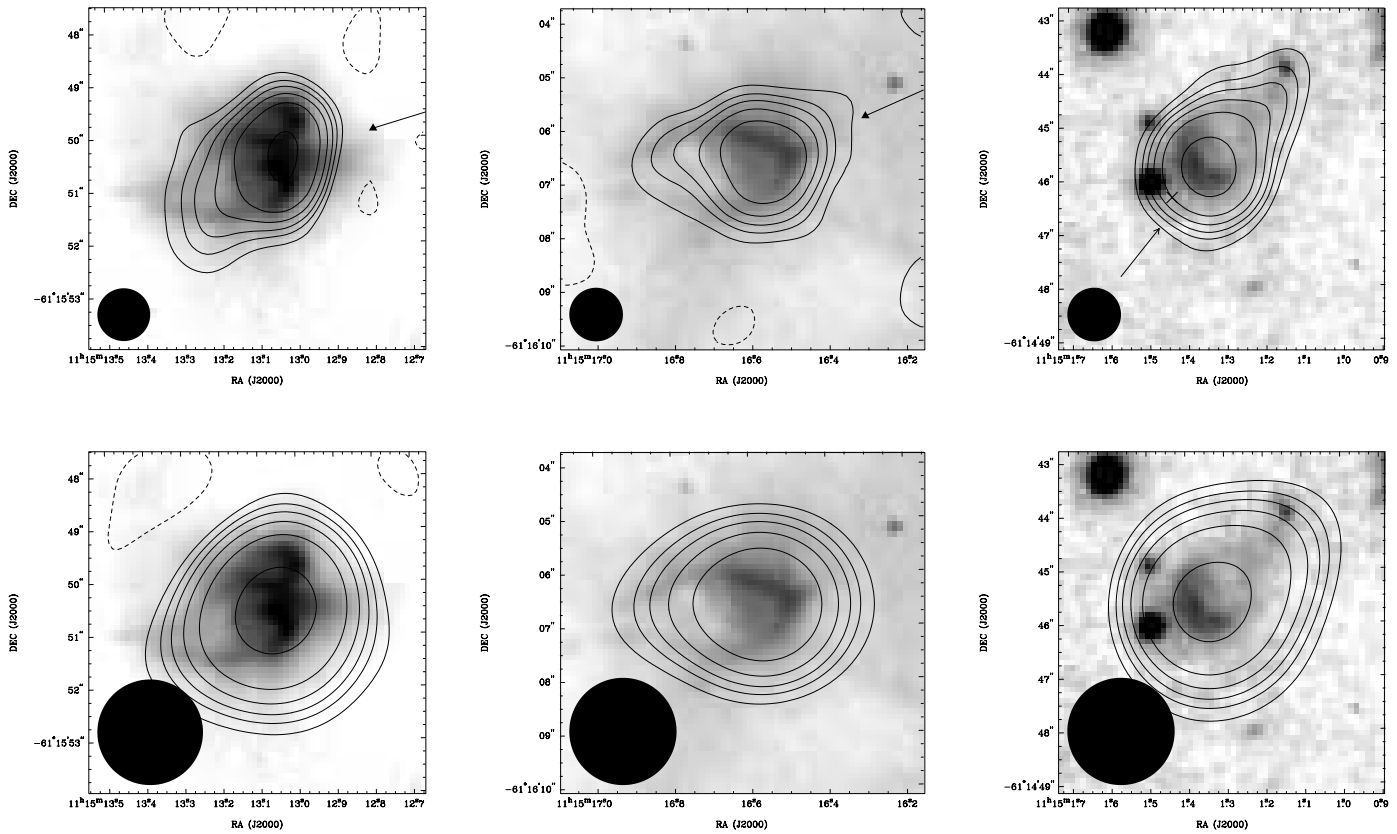

FIG. 2.—ATCA 3 cm (*top*; *u-v* cutoff at 10 kλ) and 6 cm (*bottom*; *u-v* cutoff at 25 kλ) radio-continuum contour maps of the three proplyd-like sources, numbers 1–3 from left to right, overlaid onto the Hα image from Brandner et al. (2000) for P1 and P2, and onto the *HST* broadband image for P3. The contour levels for the 3 cm maps are -0.45, 0.45, 0.75, 1.05, 1.5, 2.25, and 4.5 mJy beam^{-1}, and for the 6 cm maps they are -0.9, 0.9, 1.5, 2.1, 3.0, 4.5, and 9.0 mJy beam^{-1}. The beam is shown in the bottom left corner of each map. The Hα images have been shifted 0.″5 to the north and 0.″5 to the east in better alignment with the radio images. The arrows indicate the directions projected onto the sky from which the stellar cluster winds come. The cross near P3 indicates the position of the *Chandra* X-ray source.

3. RESULTS

The three proplyd-like sources found with the ATCA at 3 and 6 cm are clearly resolved, showing a head-tail extent of $\sim 4''$ (see Fig. 2). P3 shows the most pronounced head-tail structure, with a 3 cm flux-density ratio between head and tail of about 10 : 1. The tail is very well defined and at least $2''$ long, pointing away from the central star cluster. Unfortunately, P3 is rather faint in the low-sensitivity *HST* broadband image shown by Brandner et al. (2000); it is located outside the region of their high-sensitivity Hα image.

3.1. *Proplyd Structure and Fluxes*

The three proplyd-like objects have a cometary or head-tail shape[8] at centimeter–radio wavelengths, matching their appearance in optical images (see Fig. 2).

Integrated radio flux densities and peak fluxes are derived by summing over the whole proplyd-like object and by fitting circular Gaussians to each object. Statistical flux uncertainties are estimated as map rms times the number of beam sizes covered by the source. Depending on the method of flux determination, beam size, and *u-v* cut employed to the maps (5, 10, 15, 20, and 25 kλ), the resulting flux densities vary. The standard deviation of this variation is considered as systematic uncertainty. We found that the systematic uncertainties are always larger than the statistical error. In Table 2 we report the average fluxes and uncertainties of all three nebulae, together with their average spectral indices derived from the integrated fluxes.

Circular Gaussians[9] are used to at least attempt disentangling the head and tail structures in these cometary-shaped objects. The radio heads of the proplyd-like objects are typically $2''$–$3''$ in diameter while the total head-tail extent is $\sim 4''$. P3 shows the most pronounced head-tail structure of the three (most likely due to the viewing angle) and the smallest head (diameter $\sim 2''$) among all three proplyd-like objects, with the largest peak flux at 3 cm, while the integrated head flux is comparable. Its head-to-tail flux ratio is about 10 : 1, whereas in the other two proplyd-like objects, part of the tail may be confused with the head flux density.

Both P1 and P2 appear inclined with respect to the plane of the sky, with P1 inclined at a larger angle than P2. This can be seen in Figure 2, in which we have indicated the projected direction to the ionizing source. Figure 3 shows the residual radio-continuum image of P1 after removing a single circular Gaussian component. The residual map of P1

[8] The silhouette of proplyds has variously been referred to as cometary, tadpole, teardrop, or simply, head-tail shaped.

[9] We find that elliptical Gaussians instead of circular ones would fit too much tail flux to the head.

TABLE 2
POSITION, FLUXES AND SPECTRAL INDICES OF THE PROPLYD-LIKE OBJECTS

PARAMETER	P1		P2		P3	
	3 cm	6 cm	3 cm	6 cm	3 cm	6 cm
R.A. (J2000.0)[1]	11 15 13.042	11 15 13.058	11 15 16.557	11 15 16.579	11 15 01.336	11 15 01.330
decl. (J2000.0)	−61 15 50.38	−61 15 50.53	−61 16 06.57	−61 16 06.62	−61 14 45.69	−61 14 45.53
Peak flux (mJy beam^{-1})	4.3 ± 0.5	11.5 ± 1.6	3.2 ± 0.4	7.8 ± 1.1	5.6 ± 0.7	10.9 ± 1.4
Integrated flux[2] (mJy)	13.9 ± 1.1	18.1 ± 1.2	11.3 ± 1.4	12.1 ± 0.7	14.1 ± 1.0	16.5 ± 0.7
Spectral index of whole source[3]	-0.5 ± 0.2	-0.5 ± 0.2	-0.1 ± 0.2	-0.1 ± 0.2	-0.3 ± 0.2	-0.3 ± 0.2
$I_{H\alpha}$[4] (cm^{-2} s^{-1})	0.56	0.56	0.20	0.20	...	...
Predicted radio flux[5] (mJy)	1.56 ± 0.39	1.65 ± 0.41	0.56 ± 0.14	0.59 ± 0.15	...	...

NOTE.—Units of right ascension are hours, minutes, and seconds, and units of declination are degrees, arcminutes, and arcseconds. The position of P3 given by Brandner et al. (2000; their Table 1) contains a typographical error.

[1] Positions correspond to the radio locations of the proplyd-like object heads.

[2] The quoted 3 and 6 cm integral fluxes are derived from images with different resolution.

[3] Flux density $S_\nu \propto \nu^\alpha$, α = spectral index.

[4] Hα flux corrected for an assumed foreground extinction in Hα of $A_{H\alpha} = 4$ mag.

[5] See Brandner et al. 2000: assuming an electron temperature for the ionized gas of 10^4 K; the flux uncertainty is less than 25% due to attenuation by the neutral envelope of the proplyd-like object itself as estimated by McCullough et al. 1995 (see text).

shows two excess emission sites, one corresponding to the tail, and a second one north of it. Recent Hα images indicate that P1 is composed of two separate cometary-shaped objects (Brandner et al. 2000). We interpret the northern excess as the second head. A two-component Gaussian fit to P1 at 3 cm gives peak fluxes of 4.6 and 1.4 mJy beam^{-1} and integrated flux densities of 9.9 and 5.7 mJy for the two heads, with a separation of the two peaks of 1.″3. A two-component model could not be applied to the lower resolution 6 cm data.

The tails of all three proplyd-like objects are directed away from the star cluster, approximately coincident with the tails in Hα within the positional uncertainty of the radio/optical pointings (see Fig. 2; note the shift of 0.″5 in declination and right ascension of the *HST* image that we have employed in these figures). The uncertainty of the radio position is ~0.″15, while *HST* has a pointing uncertainty of less than 1″.

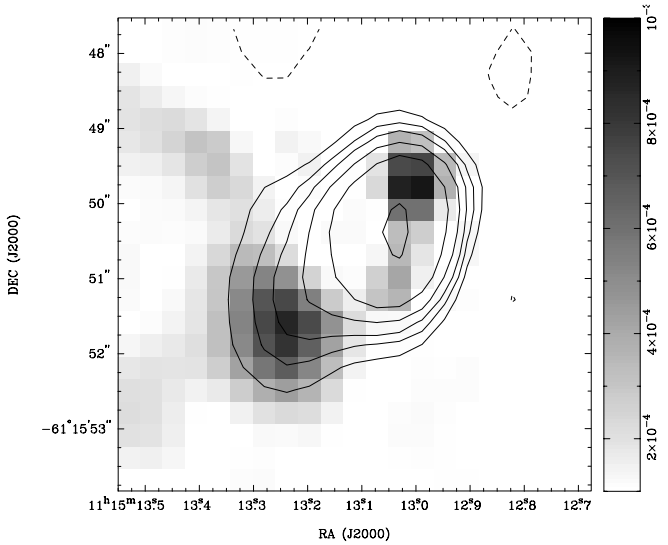

FIG. 3.—ATCA 3 cm residual image of P1 after subtracting a single circular Gaussian overlaid onto its unsubtracted brightness contour map, as shown in Fig. 2 (*top left*). The contour levels correspond to −0.3, 0.3, 0.5, 0.7, 1.0, 2.0, and 5.0 mJy beam^{-1}. P1 appears to possess two heads.

The present data were obtained in all four Stokes parameters. No polarization signal above 3 σ was detected.

Possible flux variability on timescales $\gtrsim$ days, expected from, e.g., flaring pre–main-sequence (PMS) stars with nonthermal radio spectra, cannot be tested with the present data.

3.2. *Spectral Indices of the Proplyds*

The radio-continuum fluxes (see Table 2) are a factor of 9–21 larger than those predicted by Brandner et al. (2000) assuming optically thin thermal bremsstrahlung as the radio emission mechanism (McCullough et al. 1995), which scales with the (extinction-corrected) Hα flux. The neutral part of the envelope of the proplyd-like object may attenuate Hα photons from the far side of the object depending on the viewing angle. However, McCullough et al. (1995) have estimated this effect to be less than 25% of the total Hα light for an isotropic ensemble of proplyds. Furthermore, the reasonable coincidence of the sizes of the proplyd-like objects in the radio and optical band suggests that this effect is not important here. For P1 and P3, the integrated fluxes at 6 cm are higher than those at 3 cm, whereas similar flux densities were predicted. The average spectral index of each object, shown in Table 2, is calculated on the basis of the integral fluxes at 3 and 6 cm in this table. Modeling the *u-v* distribution of the 6 cm map to match the *u-v* distribution at 3 cm gives similar results.

The average spectral indices of P1 and P3 are negative (P3 only marginally), between $\alpha = -0.5 \pm 0.2$ and -0.3 ± 0.2 ($S_\nu \propto \nu^\alpha$), indicating nonthermal emission, while the spectrum of P2 ($\alpha \approx -0.1 \pm 0.2$) is in agreement with the expectation from optically thin thermal bremsstrahlung.

Hydrodynamic simulations predict spectral indices of $\alpha \approx 0$ near the ionization fronts, which can increase up to $\alpha \approx 0.6$ when considering in addition a hydrodynamically collimated jet (S. Richling 2000, private communication). Negative spectral indices cannot be explained by this model.

Because of the high resolution and sensitivity in the radio maps, we were able to generate spectral-index maps for all three proplyd-like objects. Figure 4 shows examples of the spectral-index maps. Here we used the radio maps shown in Figure 2 and constrained ourselves to brightness densities

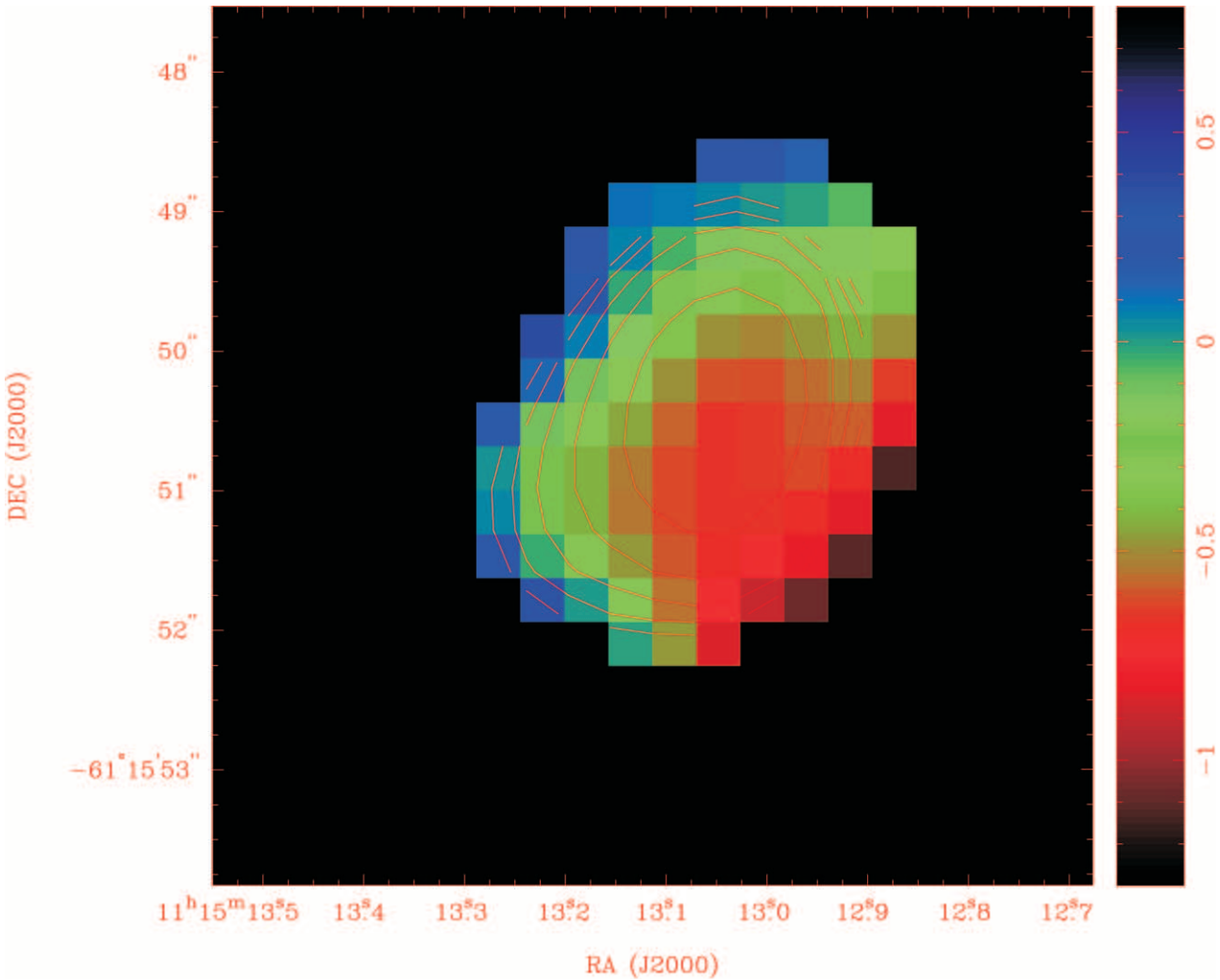

FIG. 4.—Examples of radio spectral-index maps (α; *color-coded*) with the corresponding uncertainty levels ($\Delta\alpha$; *contours*) for P1, P2, and P3 (*top to bottom*) derived from the radio maps shown in Fig. 2. The contour levels are $\Delta\alpha = 0.2$, 0.3, 0.4, 0.5, and 0.6. The 3 and 6 cm flux densities used to produce these maps have been clipped at 1.0 mJy beam^{-1}. Note the large spectral-index uncertainties at the rim of the proplyd-like objects due to the low flux densities there.

greater than 1.0 mJy beam^{-1}, which corresponds to roughly 5 σ at 6 cm and 10 σ at 3 cm (based on statistical error estimates). The radio emission zone within each proplyd-like object appears to be inhomogeneous. The spectra in at least two of the sources appear steeper in the tail than in the head, with a tendency of positive spectral indices located toward the region facing the ionizing star cluster.

3.3. *Extinction toward the Proplyds*

Melnick, Tapia, & Terlevich (1989) have derived the reddening toward NGC 3603 from *UBV* photometry and found $A_V \approx 4$–5 mag for the cluster core. However, as can be seen in their data, the visual extinction is not uniform across the whole star forming region, but increases significantly with distance from the star cluster, mainly toward the north and the south. This is confirmed by recent VLT/ISAAC data on the basis of 4750 stars, showing that the extinction can be as high as $A_V \approx 14$ mag (W. Brandner 2000, private communication). For example, star MTT 68, close to P3, has $A_V \approx 6.2$ mag, whereas star MTT 81 near P1 has $A_V \approx 4.7$ mag, and star MTT 79 close to P2 has extinction $A_V \approx 5.2$ mag. Here we use $R = A_V/E_{B-V} \approx 3.2$ as used by Melnick et al. (1989) for NGC 3603. Thus, it appears likely that P2 and P3 suffer from stronger foreground extinction than the stars in the cluster center, which have on average $A_V \lesssim 4.5$ mag.

Using the ratio between radio flux density and Hα flux as given by McCullough et al. (1995; their eq. [5]) and assuming that the radio flux density at 3 cm is dominated by thermal bremsstrahlung, we predict the Hα flux using our 3 cm radio-continuum data. The predicted fluxes are then compared with the Hα fluxes measured by Brandner et al. (2000) and used to derive lower limits for the extinction $A_{\mathrm{H}\alpha}$. (If [gyro-] synchrotron radiation dominated the radio emission, which comes from an emitting region as specified in § 4.4, the derived extinction $A_{\mathrm{H}\alpha}$ would be higher, with the exact value depending on the magnetic field.) Table 3 shows the calculated fluxes (assuming $T_e = 10^4$ K) and extinctions. Note the uncertainty in comparing different areas for which the Hα fluxes and the radio-continuum fluxes have been obtained. Brandner et al. (2000) give the Hα surface brightness of the proplyd-like object heads, measured for a 0.″5 aperture radius, whereas we quote peak fluxes per beam where the beam size is $\sim 1.''0 \times 1.''0$. For $A_{\mathrm{H}\alpha} \approx 0.85 A_V$, we find $A_V \approx 6.0$ for P1 and $A_V \approx 6.7$ for P2. We thus find sig-

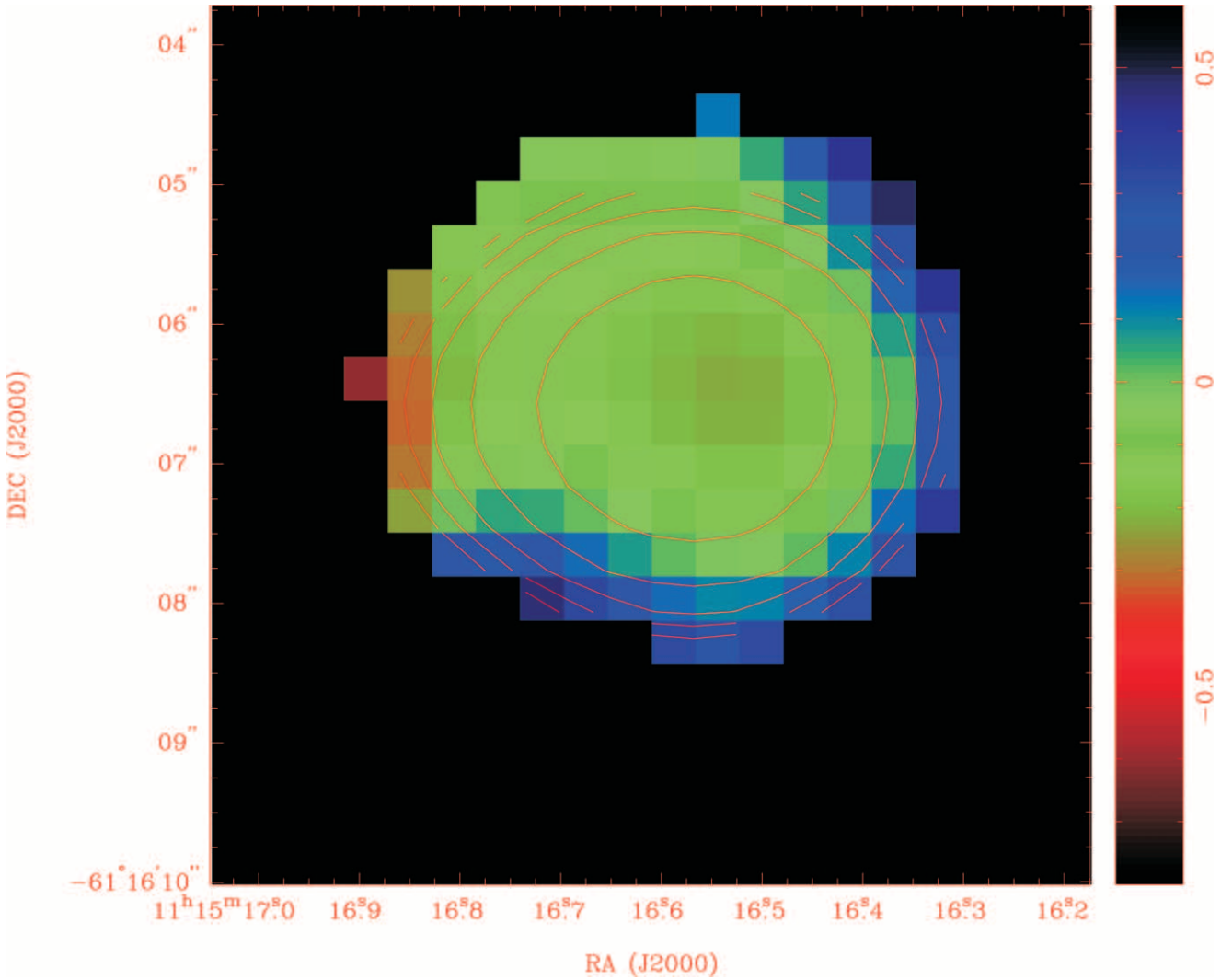

FIG. 4.—*Continued*

nificant excess extinction for both proplyd-like objects, which may be intrinsic to the proplyd-like objects themselves; otherwise, the extinction estimate derived from the stars is underestimated.

3.4. *Proplyd Densities and Mass-Loss Rates*

Estimates for the electron/ion density inside the heads can be obtained from our radio data if thermal bremsstrahlung dominates the radio emission. This is likely to be the case for P2 and maybe P3, while for P1, the derived values should be considered as upper limits. The bremsstrahlung intensity in the radio domain for a thermal, ionized H gas of constant density in a sphere is (Mezger & Henderson 1967)

$$S_{\rm radio} \approx 1.9 D_{\rm kpc} f_{\rm th} \theta_{\rm sec}^3 N_{e,4} N_{\rm ion,4} \nu_{\rm GHz}^{-0.1} T_4^{-0.35} \ {\rm mJy} \ ,$$

where $D_{\rm kpc}$ is the source distance in kpc, $\theta_{\rm sec}$ is the apparent radius of the source in arcseconds, $N_{e,4}$ and $N_{\rm ion,4}$ are the densities of the thermal electrons and ions, respectively, in 10^4 cm^{-3}, $\nu_{\rm GHz}$ is the observing frequency in GHz, and T_4 is the electron temperature of the ionized gas in 10^4 K. The quantity $f_{\rm th}$ is the ratio of thermally emitting–to-total volume of the source and is introduced to account for the possibility of smaller emitting volumes than the apparent extent of the source. This is likely because only the outermost layers in proplyds are believed to be ionized. We estimate the proplyd heads to be $\sim$2″–3″ in diameter. For $T_4 = 1$ and $N_e \approx N_{\rm ion}$, we estimate the electron density by comparing the expected radio flux with the observed 3 cm proplyd head flux densities and find $N_e = (9, 7, \text{and } 13) \times 10^3 f_{\rm th}^{-1/2}$ cm^{-3} for P1, P2, and P3, respectively. [The corresponding emission measures are EM $= (5.9, 3.5, \text{and } 9.3) \times 10^6 f_{\rm th}^{-2/3}$ cm^{-6} pc.] If the emitting volume is smaller than the total source volume, the electron density and emission measure increase accordingly. From spectral considerations, the emission must be optically thin, i.e., free-free absorption may set in at frequencies lower than 4.8 GHz. Thus, values of EM cannot exceed $\sim$several $\times 10^7$ cm^{-6} pc, in order to avoid free-free absorption at frequencies above 4.8 GHz. This constrains the size of the thermally emitting volume of the three proplyd-like objects to at least 4%, 2%, and 9% of the total source volumes, and consequently puts limits on the thermal electron densities in the sources: (4.5, 4.9, and 4.3) $\times 10^4$ cm^{-3} for P1, P2, and P3, respectively. Note that these numbers should be considered as upper limits if the observed radio flux is dominantly of nonthermal origin. These numbers are in reasonable agreement with $N_e \geq 10^4$ cm^{-3}, derived from [S II] line ratios by Brandner et al.

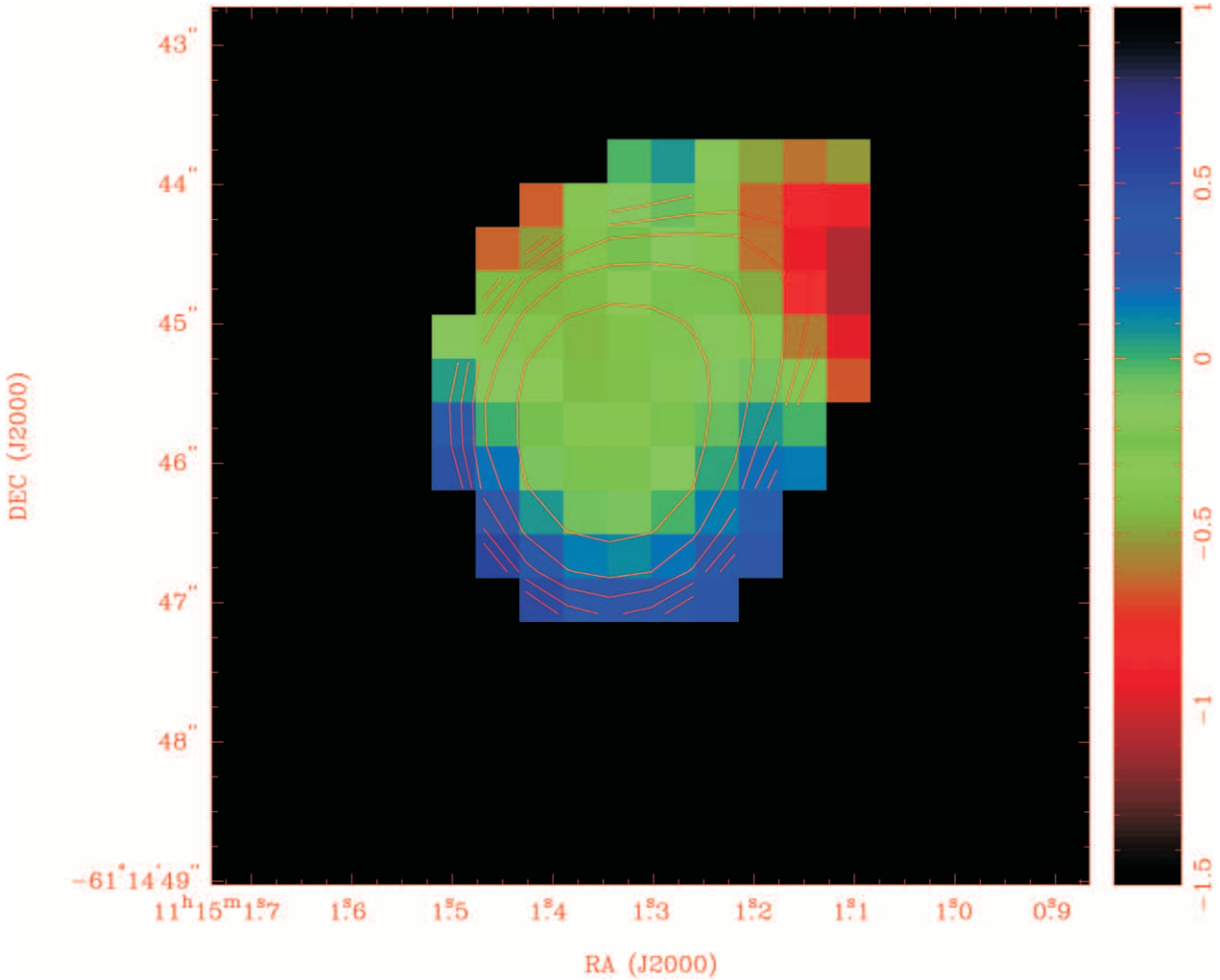

FIG. 4.—*Continued*

(2000). For the Ori proplyds, densities of the order of 10^5–10^6 cm^{-3} have been found (Henney & O'Dell 1999). Note that our derived numbers suffer from uncertainties due to the unknown geometrical projection angle of the proplyd-like objects and hence the true source diameters.

Mass loss from the proplyd-like objects occurs through external heating of the envelope by the far-ultraviolet (FUV) radiation field from hot stars, especially from the core of NGC 3603, and subsequent evaporation. Knowing the electron density, the mass-loss rate in a wind is given by $\dot{M} = 4\pi R^2 N_e \mu m_{\rm H} v_W$, with R the system radius, $m_{\rm H}$ the ion mass, and v_W the evaporation velocity. Assuming a pure hydrogen gas, $\mu = 1.3$, we find $\dot{M}/v_{20} \approx (5\text{–}10) \times 10^{-5}\ M_\odot$ yr^{-1} for the heads of all three proplyd-like objects, where v_{20} is the wind velocity in units of 20 km s^{-1}. Brandner et al. (2000) found evaporation flow velocities of the order of 10–25 km s^{-1}. The derived upper limits for the mass-loss rates are of the same order as estimated by Brandner et al. (2000) and about 2 orders of magnitude higher than the typical values for the Ori proplyds.

A rough estimate of the mass reservoir of the NGC 3603 proplyd-like objects can then be derived by multiplying the mass-loss rate with an estimated evaporation timescale of $\sim 10^5$ yr (Brandner et al. 2000). This gives a mass for the proplyd-like objects of the order of 1–10 $M_\odot$, 10–1000 times larger than for the Ori proplyds. The radius of the putative disks in these massive objects can be estimated using the evaporation model of Johnstone et al. (1996), which considers the mass reservoir in a disklike shape. We find an approximate disk radius of 2000 AU ($\approx 0\farcs3$) for all three NGC 3603 proplyd-like objects: Brandner et al. (2000) found $\sim$3400 AU from hydrodynamical simulations.

TABLE 3
FLUXES AND DERIVED EXTINCTION

PARAMETER	PROPLYD 1	2	3
3 cm peak flux (mJy beam^{-1})	4.3	3.2	5.6
Predicted Hα peak flux (cm^{-2} s^{-1})	1.5	1.1	2.0
Derived $A_{\rm H\alpha}$ (mag)	5.1	5.7	...

4. DISCUSSION

4.1. *Comparison with the Proplyds in the Orion and Lagoon Nebulae*

The proplyd-like objects in NGC 3603 are 20–30 times larger and much more spectacular than those in Ori, which

were detected at 2 and 20 cm with the Very Large Array (VLA) (see McCullough et al. 1995, and references therein; Henney & O'Dell 1999).

Ori contains numerous dense clumps, originally classified as UCHRs, but now known to be proplyds. Most Ori proplyds have central disks, sometimes seen only in silhouette against the background light. In recent *HST* images, dozens of jets powered by young stars embedded in proplyds have been found (Bally et al. 2000). All Ori proplyds detected at radio wavelengths are nonvariable thermal emitters with spectral indices between −0.1 and 0.2 (Felli et al. 1993) and located within 0.04 pc of the dominant ionizing O star (θ^1 Ori C). The nonthermal Ori radio sources show strong variability and are mostly associated with visible PMS stars. Their nonthermal spectra are usually explained as being due to stellar flaring activity.

G5.97−1.17 ($D = 1.8$ kpc) was originally classified as a UCHR but is now thought to be a proplyd at ∼5000 AU projected distance from the O7 star Herschel 36 in the center of M8, the Lagoon Nebula (Stecklum et al. 1998). ESO NIR, *HST* optical, and VLA radio-continuum observations indicate that G5.97−1.17 is a young star surrounded by a circumstellar disk that is likely being photoevaporated by Her 36, similar to the proplyds in Ori. The previous hypothesis suggested that G5.97−1.17 was a UCHR intrinsically ionized by an embedded B0 star. However, Stecklum et al. (1998) showed that G5.97−1.17 is predominantly externally ionized, and thus the spectral type of the embedded star should be later than B5. The Hα flux over 0.″6 is consistent with the $\lambda = 2$ cm appearance. Optical and NIR continuum images show that the central star is displaced from the peak of the bow shock by 0.″125. NIR photometry of G5.97−1.17 revealed that its central star is extremely red, which cannot be explained by extinction laws that use spherical matter distributions. This supports the idea of the circumstellar matter surrounding the central star of G5.97−1.17 being arranged as a disk. The centimeter–radio spectrum of G5.97−1.17 appears flat, which is interpreted as optically thin free-free emission (Wood & Churchwell 1989; Doherty et al. 1994). No OH or H_2O masers, which are often associated with UCHRs, are known in G5.97−1.17.

In comparison, the NGC 3603 proplyd-like objects appear rather peculiar and spectacular. Not only are they the largest and most massive ones found so far, but exposed to an extremely strong FUV radiation field, they also suffer the largest mass losses, although their distances from the ionizing source are larger than for the Orion or Lagoon Nebula proplyds. No embedded source or disk has been found for any of the NGC 3603 proplyd-like objects. At centimeter wavelengths, they are so far the only proplyd-like objects showing nonthermal radio emission.

The spatial distribution of the NGC 3603 proplyd-like objects is also peculiar. Not only are they apparently distributed along a straight line (see § 4.3 for further discussion), but all three also lie clearly to the north of the ionized gas region and avoid the region northeast and southwest from the stellar cluster. This is in contrast to the Ori proplyds, which do not appear to be located in preferred regions of the nebula (e.g., Bally et al. 2000). Since sequential star formation proceeding from north to south seems evident in NGC 3603 (e.g., De Pree et al. 1999), this suggests that the proplyd-like structures in this region might have emerged just recently.

4.2. *External versus Internal Ionization*

A possible way to prove that the proplyd-like objects have indeed been ionized *externally* by the star cluster is to show that the observed radio fluxes for the proplyd-like objects are consistent with the number of ionizing photons they receive from the cluster stars. For simplicity, we assume thermal radio emission and note that this leads to an upper limit for the number of ionizing photons needed to produce the observed radio flux density. In this case, the brightness temperature is directly proportional to the number of ionizing photons. Because NGC 3603 contains a large number of stars that are extremely hot and luminous, they provide an ionizing flux that is several orders of magnitude larger than that in Ori or M8 (see Table 4). The expected brightness temperatures at the projected distances of 1.3, 2.2, and 2.0 pc of the proplyd-like objects from the ionizing source due to a Lyman flux of 10^{51} photons s^{-1} (Brandner et al. 2000) are 200, 70, and 90 K at 3 cm, assuming $T_4 = 1$. This is only slightly higher than our estimates derived from the ATCA 3 cm maps of 40, 30, and 70 K for the three proplyd-like objects, respectively. We can also compare the number of ionizing photons required to deliver the observed flux densities at the location of the proplyd-like objects and compare this number with the number of Lyman photons they receive from the star cluster. Noting that the proplyd-like objects subtend a fraction (6, 3, and 2) $\times 10^{-5}$ of the total solid angle seen by the cluster stars, they thus receive (6, 3, and 2) $\times 10^{46}$ photons s^{-1}, respectively. On the other hand, the required number of ionizing photons at the location of each proplyd-like object to deliver the observed radio flux density is about 2×10^{46} photons s^{-1} in all three cases. These comparisons show that the number of required Lyman photons is slightly lower than that provided by the star cluster, and thus would even allow an additional dust attenuation and/or, more likely, longer linear distances between the proplyd-like objects and the ionizing source in the external ionizing scenario. Significant ionizing power from within the proplyd-like objects appears therefore unlikely, which puts the spectral type of any central stars to later than ∼B1, and hence the mass to below $\sim 10\ M_\odot$.

4.3. *Do the Proplyd-like Objects Host Disks?*

The present radio data as well as the recently published *HST*/VLT images do not provide any direct evidence that the observed proplyd-like objects in NGC 3603 host any (proto-) stellar objects or disks. To a limiting K_s magnitude of 18, no circumstellar disk or central stellar object in any of the three proplyd-like objects has been detected by *HST*/VLT observations. Instead, the cometary-shaped nebulae may rather be massive emission regions photoionized by the radiation from the star cluster. Mellema et al. (1998) have presented model calculations for such clumps, called fast low-ionization emission regions (FLIERs) or ansae, which are commonly located along the major axis toward the ionizing source. Indeed, all three proplyd-like objects apparently lie approximately along one straight line, with the outflow source Sher 25 located roughly midway between P1 and P3. Although the bipolar outflow from Sher 25 appears not to point in the direction of any of the three proplyd-like sources, the ringlike structure around Sher 25, roughly perpendicular to its jet, has been shown to expand with a velocity of ∼30 km s^{-1} (Brandner et al. 1997) and could in principle be related to the origin of the proplyd-like clumps.

TABLE 4
COMPARISON WITH OTHER KNOWN PROPLYDS[1]

Parameter	M42 (Orion Nebula)	M8, NGC 6523 (Lagoon Nebula)	NGC 3603
Distance (kpc)	0.45	1.8	6.1
Central star(s)	Θ^1Ori C	Herschel 36	Cluster
Star type(s)	O7	O7.5 V	3 WNs + ~70 O stars
$L_{bol}(L_\odot)$	$\sim 10^5$	$\sim 10^5$	2×10^7
Lyman flux (photons s^{-1})	$\sim 8 \times 10^{48}$	2×10^{48}	10^{51}
Extinction (mag)	4–6	~5	4–6
Masers	H_2O, SiO	...	OH, H_2O, CH_3OH
Number of proplyds	> 150	1 = G5.97–1.7	3
Head size (AU)	45–355	1080	7200–10800
Distance to central stars (pc)	0.01–0.15	0.024	1.3, 2.2, 2.0
Radio flux (mJy)	0.3–1.4	17	10–12
Brightness temperature (K)	$\sim 10^2$–10^3	~1500	30–90
Emission measure[2] (pc cm^{-6})	8×10^6	$(0.3–2) \times 10^8$	$(3–9) \times 10^6 f_{th}^{-2/3}$
Electron density (cm^{-3})	10^5–10^6	$(4–20) \times 10^4$	$\sim 10^4$
Mass-loss rate ($M_\odot$ yr^{-1})	1.2×10^{-7}	7×10^{-7}	10^{-5}
Bow-shock distance (AU)	~100	540	44400, 17400, ...
Velocity (km s^{-1})	~10–15	~10	10–25
Evaporation timescale (yr)	$\sim 10^4$	$\sim 10^5$	$\sim 10^5$
Proplyd mass ($M_\odot$)	0.01–0.1	~0.1	~1–10
Disk radius (AU)	27–175	160	3400
Disk mass ($M_\odot$)	$\sim (0.5–20) \times 10^{-3}$	$\sim 6 \times 10^{-2}$	...
References	1, 2	3	4

[1] Detailed information on the NGC 2024 proplyd is not available.
[2] For NGC 3603, see § 3.4.
REFERENCES.—(1) Henney & O'Dell 1999; (2) McCullough et al. 1995; (3) Stecklum et al. 1998; (4) Brandner et al. 2000.

In addition, models such as the FLIER model that are not based on disklike mass distributions typically give short evaporation times, inconsistent with the distance of the proplyd-like objects from Sher 25 (W. Brandner 2001, private communication) and the approximate date of the mass-loss event about 6630 yr ago in Sher 25 (Brandner et al. 1997). Thus, the existence of such features at large distances from the cluster center appears to favor models in which most of the material is concentrated in compact structures such as disks. The actual presence of disklike structures is, however, not confirmed.

4.4. *The Possible Origin of the Nonthermal Emission*

The significantly nonthermal spectrum ($\alpha \ll 0$, $S_\nu \propto \nu^\alpha$) from at least one of the three NGC 3603 proplyd-like objects (P1; P3 seems to be marginally nonthermal) appears to be steepest ($\alpha < -0.5$) in the tail, slightly flatter ($\alpha = -0.5$ to 0.1) in the head, and have a tendency of positive spectral indices ($\alpha > 0$) located toward the region facing the ionizing star cluster rather than away from it. This is not expected from nonthermal radio emission from a wind-wind collision region. The nonthermal radiation must originate rather from inside the proplyd-like objects, either from their putative central stars hidden behind thick material, the surrounding disks, or the envelopes. A stellar origin analogous to active star coronal emission seems to be unlikely because of the extended nature of the observed source. Nonthermal radio spectra could be produced by a population of energetic particles emitting synchrotron, gyrosynchrotron, or gyroresonance radiation in a magnetic field. For gyrosynchrotron radiation, the emission is concentrated at harmonic numbers $s = \nu/\nu_B = 10$–100 (where $\nu_B \approx 2.8 \times 10^{-3} B_G$ GHz is the gyrofrequency and B_G is the magnetic field strength in Gauss), and thus magnetic field strengths of the order of $B \approx 20$–200 G are required. These high field values cannot be present in extended sources, which leaves synchrotron radiation as the only plausible emission mechanism.

Disk or envelope, whatever the ultimate source might be, the negative spectral indices suggest optically thin nonthermal processes as the dominant radiation mechanism in P1, and maybe P3. One could argue that the shock created by the evaporation flow predicted in proplyd models could accelerate charged particles within the objects. Other possibilities may be inflow-outflow activity causing shocks during the early stage of star formation, compression and reconnection of magnetic fields in the collapsing envelope, or magnetic reconnection in star-disk interactions in YSOs leading to production of energetic particles. Magnetic fields are known to exist in molecular clouds (Crutcher 1999), and therefore it appears plausible that gas clumps still contain "fossil" fields. In a magnetized plasma, acceleration due to particle collisions and subsequent bremsstrahlung can often be negligible in comparison with acceleration due to gyration around the field lines. In place of free-free emission, there is then synchrotron emission from energetic particles. The negative radio spectral indices in P1 and P3 are conveniently explained by nonthermal particle spectra. Because thermal bremsstrahlung is proportional to $N_e^2 T_e^{-1/2}$ and synchrotron emission is proportional to $N_e B^\beta$ ($\beta > 0$), the former dominates if the density is high enough, or if the temperature or field strength is low enough. Indeed the electron densities found in the NGC 3603 proplyd-like objects are ~2 orders of magnitude smaller than in the Ori proplyds (see Table 4). The different energy dependencies of the two kinds of emission may lead to one dominating at low frequencies and the other at high frequencies.

A lower limit for a possible magnetic field is given by the Razin-Tsytovich effect. In order to avoid a Razin-suppression of the radio spectrum above $\lambda = 6$ cm, the magnetic field cannot be smaller than $\sim 10^{-5}$ G for an electron density of 10^4 cm^{-3} in the emission region. On the other hand, to avoid gyroresonance absorption above $\lambda = 6$ cm, the field strength cannot be higher than 10^3 G. The equipartition magnetic field, the minimum possible value in flare loops, for a $T_e = 10^4$ K particle distribution with density 10^4 cm^{-3} is $\sim 10^{-3}$ G. Note that synchrotron photons of energy 4.8 GHz in a 10^{-5} G field must have been produced by ~ 10 GeV electrons. Efficient particle acceleration may occur, e.g., at the proplyd surface, from flow amplification of even very weak ambient magnetic fields followed by local reconnection events (e.g., Shore & Larosa 1999).

The flux density due to synchrotron radiation from a homogeneous sphere with diameter l in a uniform field and with a low energy cutoff $E_{\rm min,MeV}$ in units of MeV of the particle distribution $E^{-\alpha_e}$, with $\alpha_e = 2$ spectral index,[10] is given by (e.g., Dulk 1985)

$$S_{\nu,\rm syn} \approx 5 \times 10^{18} N_{e,\rm nt,4} B_{\rm G}^{1.5} E_{\rm min,MeV} l_{\rm pc}^{3} D_{\rm kpc}^{-2} \nu_{\rm GHz}^{-0.5} \ \rm mJy \ .$$

The nonthermal electrons might have been energized by, e.g., shock acceleration or magnetic reconnection events, out of the pool of thermal particles, or they may be Galactic cosmic rays penetrating the star forming region. In the latter case, $N_{e,\rm nt} \approx 10^{-2}$ to 10^{-1} cm^{-3} and $\alpha_e \approx 2.4$, and thus $B \approx 10^{-3}$ G (for $E_{\rm min,MeV} = 1$). For the former case, because energy is conserved, the production efficiency of the high-energy particles is related to the properties of the thermal background particles, and vice versa. Realistic nonlinear diffusive particle acceleration scenarios typically yield $N_{e,\rm nt}/N_e \sim 10^{-5}$ to 10^{-1} (i.e., the fraction of total electrons that end up with high energies; e.g., Ellison, Bereshko, & Baring 2000), while magnetic reconnection might be as efficient as $N_{e,\rm nt}/N_e \sim 0.01$ for the present densities and temperature (Tandberg-Hanssen & Emslie 1988). Since the thermal electron density N_e cannot be significantly smaller than $\approx 10^4$ cm^{-3} (derived from [S II] line ratios; see § 3.4), and $N_{e,\rm nt} \leq N_e$ if thermal and nonthermal electrons have the same source, we find that the size of the actual magnetized volume emitting nonthermal radiation must be smaller than the appearance of the proplyd-like object on the sky for this case. If particle trapping is at work, $N_{e,\rm nt} \geq N_e$ is possible, and consequently, the ratio of emitting-to-total volume of the proplyd-like object becomes even smaller.

The present data, however, do not allow us to quantitatively constrain the actual size of the source responsible for the nonthermal radiation.

We note that the recent discovery of variable X-ray emission from some proplyds in Ori by Schulz et al. (2001) support the idea of a nonthermal emission volume smaller than the appearance of the proplyd-like object on the sky. The size of the emitting region was estimated on the basis of variability arguments to be of the order of 1–10 AU.

[10] Shock acceleration typically predicts an E^{-2} power law, which we use as a reasonable assumption here.

5. SUMMARY AND CONCLUSIONS

The three massive ($\sim$1–10 $M_\odot$) proplyd-like nebulae in NGC 3603, which have recently been discovered by Brandner et al. (2000), have been clearly detected and resolved with the ATCA at 3 and 6 cm, with one of them likely to be composed of two cometary-shaped objects. Their flux densities are about 10–20 times higher than expected from the Hα measurements, and a nonthermal average spectrum can be associated with at least one of the three proplyd-like sources. This is the first time that nonthermal radio emission has been detected from proplyd-like sources. Our spectral-index maps show that the emission region is rather inhomogeneous, with negative spectral indices in the tail and part of the head, whereas positive spectral indices, indicating thermal free-free emission, tend to be detected from a small region facing the star cluster.

We derive upper limits for the mass-loss rates of 10^{-5} $M_\odot$ yr^{-1} and electron densities of 10^4 cm^{-3}. These are in reasonable agreement with estimates from recent *HST* images.

We show that synchrotron emission from a magnetized, relativistic, nonthermal particle population may explain the nonthermal spectral regions. Energetic electrons necessary for synchrotron radiation may be produced through shocks or by magnetic reconnection out of the pool of thermal particles, or may be Galactic cosmic rays.

A stellar origin of the observed flux densities appears unlikely considering that the sources are extended. Thus, magnetic fields, which have been neglected in proplyd models so far, are possibly associated with the proplyd envelopes or disks and appear to be crucial in understanding the physical processes in these proplyd-like objects.

Melnick et al. (1989) have shown that an inhomogeneous dust distribution in NGC 3603 causes increasing extinction with distance from the star cluster. In particular, the extinction at the location of the proplyd-like objects is estimated to lie between $A_V \approx 5$–6 mag. Extinction estimates derived from the radio-to-Hα luminosity ratio are 1–2 mag higher.

The ultimate discovery of the so-far undetected disks, which are thought to be part of all proplyds, would give important hints about the origin of the extremely high and nonthermal radio fluxes and the nature of the cometary-shaped clumps seen in NGC 3603. This may be accomplished in future millimeter observations with an upgraded ATCA.

We are grateful to Wolfgang Brandner for providing the *HST* image of NGC 3603 to overlay on our radio images, for interesting discussions, and for carefully reading the manuscript. We thank Jessica Chapman, Jim Caswell, Simon Johnston, Tylor Bourke, and Sergey Marchenko for reading the manuscript and for many constructive comments that improved our paper significantly. A. M. acknowledges a postdoctoral bursary from the Quebec Government. A. F. J. M. thanks NSERC (Canada) and FCAR (Quebec) for financial support. I. R. S. acknowledges the receipt of a PPARC Advanced Fellowship.

REFERENCES

Bally, J., O'Dell, C. R., & McCaughrean, M. J. 2000, AJ, 119, 2919
Brandner, W., Chu, Y.-H., Eisenhauer, F., Grebel, E. K., & Points, S. D. 1997, ApJ, 489, L153
Brandner, W., et al. 2000, AJ, 119, 292
Churchwell, E. 1990, A&A Rev., 2, 79
Crowther, P. A., & Dessart, L. 1998, MNRAS, 296, 622
Crutcher, D. 1999, ApJ, 520, 706
De Koter, A., Heap, S. R., & Hubeny, I. 1997, ApJ, 477, 792
De Pree, C. G., Nysewander, M. C., & Goss, W. M. 1999, AJ, 117, 2902
Doherty, R. M., Puxley, P., Doyon, R., & Brand, P. W. J. L. 1994, MNRAS, 266, 497
Dulk, G. A. 1985, ARA&A, 23, 169
Ellison, D. C., Berezhko, E. G., & Baring, M. G. 2000, ApJ, 540, 292
Felli, M., Taylor, G. B., Catarzi, M., Churchwell, E., & Kurtz, S. 1993, A&AS, 101, 127
Henney, W. J., & O'Dell, C. R. 1999, AJ, 118, 2350
Johnstone, D., Hollenbach, D., Störzer, H., Bally, J., Devine, D., & Southerland, R. 1996, BAAS, 189, 49.12
McCullough, P. R., et al. 1995, ApJ, 438, 394
Mellema, G., Raga, A. C., Canto, J., Lundquist, P., Balick, B., Steffen, W., & Noriega-Crespo, A. 1998, A&A, 331, 335
Melnick, J., Tapia, M., & Terlevich, R. 1989, A&A, 213, 89
Mezger, P. G., & Henderson, A. P. 1967, ApJ, 147, 471
Moffat, A. F. J., Drissen, L., & Shara, M. 1994, ApJ, 436, 183
O'Dell, C. R., Wen, Z., & Hu, X. 1993, ApJ, 410, 696
Schulz, N. S., Canizares, C., Huenemoerder, D., Kastner, J. H., Taylor, S. C., & Bergstrom, E. J. 2001, ApJ, 549, 441
Shore, S. N., & Larosa, T. N. 1999, ApJ, 521, 587
Stapelfeldt, K., Sahai, R., Werner, M., & Trauger, J. 1997, in ASP Conf. Ser. 199, Planets Beyond the Solar System and the Next Generation of Space Missions, ed. D. Soderblom (San Francisco: ASP), 131
Stecklum, B., Henning, T., Feldt, M., Hayward, T. L., Hoare, M. G., Hofner, P., & Richter, S. 1998, AJ, 115, 767
Tandberg-Hanssen, E., & Emslie, A. G. 1988, in The Physics of Solar Flares (New York: Cambridge Univ. Press)
Wood, D. O. S., & Churchwell, E. 1989, ApJS, 69, 831